CHALMERS
UNIVERSITY OF TECHNOLOGY

Enhanced oxygen reduction activity with rare earth metal alloy catalysts in proton exchange membrane fuel cells

Electrochimica Acta 387 (2021) 138454

Contents lists available at ScienceDirect

Electrochimica Acta

journal homepage: www.elsevier.com/locate/electacta

Enhanced oxygen reduction activity with rare earth metal alloy catalysts in proton exchange membrane fuel cells

Björn Eriksson[a,*], Gerard Montserrat-Sisó[b], Rosemary Brown[b], Tomáš Skála[c], Rakel Wreland Lindström[a], Göran Lindbergh[a], Björn Wickman[b], Carina Lagergren[a]

[a] Applied Electrochemistry, Department of Chemical Engineering, School of Engineering Sciences in Chemistry, Biotechnology and Health, KTH Royal Institute of Technology, Stockholm, SE 10044, Sweden
[b] Division of Chemical Physics, Department of Physics, Chalmers University of Technology, Gothenburg, SE 41296, Sweden
[c] Faculty of Mathematics and Physics, Department of Surface and Plasma Science, Charles University, V Holešovičkách 2, Prague, CZ 18000, Czech Republic

ARTICLE INFO

Article history:
Received 18 December 2020
Revised 2 April 2021
Accepted 20 April 2021
Available online 25 April 2021

Keywords:
Proton exchange membrane fuel cell
Platinum rare earth metal alloy
Oxygen reduction reaction

ABSTRACT

Alloying platinum is an approach to increase the oxygen reduction reaction (ORR) activity and at the same time reduce the amount of precious platinum catalyst in proton exchange membrane fuel cells (PEMFC). In this work the cathode activity of thin films of rare earth metals (REM) alloys, Pt_3Y, Pt_5Gd and Pt_5Tb, produced by sputter deposition onto gas diffusion layers, are evaluated in a fuel cell by means of polarization curves in O_2/H_2, and cyclic- and CO-stripping voltammetry in $N_2/5\%$ H_2. Prior to evaluation, the model electrodes were acid-treated to obtain a Pt skin covering the PtREM alloy bulk, as was revealed by energy-dispersive X-ray spectroscopy (EDX) and X-ray photoelectron spectroscopy (XPS). The core shell alloys of Pt_3Y and Pt_5Gd catalysts show a specific activity enhancement at 0.9 V of 2.5 times compared to pure Pt. The slightly lower enhancement factor of 2.0 for Pt_5Tb is concluded to be due to leaching of the REM, that resulted in a thicker, and subsequently less strained, Pt overlayer. The high activity, combined with the minor changes in surface composition, achieved in the fuel cell environment shows that PtREM core shell catalysts are promising for the cathode reaction in PEMFC.

1. Introduction

For a sustainable energy society, not relying on combustion of fossil fuels, fuel cells will be important alternatives, especially within the transport sector, where high energy density is necessary. For fuel cells to reach full scale commercialization, a reduction of total cost is required [1]. One of the most expensive components in proton exchange membrane fuel cells (PEMFC) is the platinum catalyst.

High amounts of platinum catalyst are required for the sluggish oxygen reduction reaction (ORR). One approach to decrease the amount of platinum is to develop more active catalysts. While platinum is an efficient catalyst for ORR, it is not optimal. The kinetics of the ORR on platinum catalysts are limited by the strong OH binding energy, and by lowering the binding energy of OH on Pt(111) by approximately 0.1 eV, the activity could be increased by an order of magnitude [2,3]. The binding energy can be shifted by introducing an alloying material. This has been achieved with transition metals, such as Ni and Co, resulting in an increase in mass activity, compared to pure platinum, of an order of magnitude in rotating disk measurements (RDE) [4–10]. However, transition metal alloys are not completely stable in PEMFC, and can dealloy [8,11–13], leading to a decrease in activity with time and usage.

Alloying Pt with a rare earth metal (REM) is a promising alternative to PtNi and PtCo catalysts. Due to the more negative energy of formation of the alloy, the REM should be more energetically favored to stay in the bulk, which should increase the stability compared to platinum alloys with late transition metals [3]. Several PtREM materials have been tested in RDE [2,14–20]. For these the activity increase has been reported to be between 6 and 7 times the specific activity of pure platinum, and up to an order of magnitude in mass activity, compared to platinum nanoparticles. Further, the cost of REM-oxides are several orders of magnitude lower and their abundance several orders of magnitude higher than that of Pt [21]. However, even if the alloy catalysts perform well in RDE it is not certain that the same activity increase will be found in a fuel cell, as the conditions in RDE are not comparable with the PEMFC environment.

* Corresponding author.
E-mail address: bjorerik@kth.se (B. Eriksson).

https://doi.org/10.1016/j.electacta.2021.138454

In our previous study in a real fuel cell setup, we found that model electrodes with sputtered thin films of Pt_3Y in contact with a Nafion membrane had approximately double the activity compared to sputtered platinum [22], however still less active than proven in RDE experiments. Part of the reason why the Pt_3Y films were less active in the fuel cell than in RDE experiments is likely due to the fact that they were sputtered on to the microporous layer (MPL) of the gas diffusion layer (GDL), leading to uneven and non-optimal structure of the alloy. However, it is still not clear if this accounts for the whole difference in activity or if there are processes specific to the fuel cell environment that are mainly responsible. Previous studies with Pt_3Y in fuel cells have shown increase in specific activity by a factor between 2 and 3 compared to Pt/C [23,24]. It is also of great interest to see if other PtREM alloys, which display high activity in RDE, perform similarly under real fuel cell conditions [15].

In this study, thin film electrodes based on Pt_3Y, Pt_5Gd and Pt_5Tb are evaluated and compared in a PEMFC in a similar manner as in our previous work [22]. The thin-film electrodes can be seen as a two-dimensional model electrode used to study new catalyst in a more realistic fuel cell environment than for instance acid solutions used for RDE measurements. From a pure catalytic perspective, thin-film electrodes allow for more accurate determination of oxygen reduction activity compared to a porous electrode, as effects from local mass transport, potential and humidity will not affect the electrodes to the same extent. The film thickness of 60 nm was chosen to give a relatively robust film. The MPL support was considered porous enough for sufficient supply of oxygen. Pt_3Y was chosen due to its high performance in our previous study [22], while Pt_5Gd and Pt_5Tb were chosen due to their reported high performance in RDE studies [2,14,25]. Physical characterization of the samples confirms the formation of a Pt overlayer after acid treatment, which leads to an increase in electrochemical activity. The overlayer and activity persists throughout the electrochemical testing, showing that these alloys are stable during fuel cell operation. These results highlight that PtREM catalysts are active and stable in an operating fuel cell.

2. Experimental

2.1. Sputter deposition of alloy catalysts

Thin films of Pt, Pt_3Y, Pt_5Tb and Pt_5Gd were deposited using single pure metal or alloy targets (from Goodfellow) using magnetron sputtering in a Nordiko 2000 sputter coater onto the MPL of the GDL (Carbel Cl). The base pressure of the sputtering system was lower than 1.0×10^{-6} mbar and sputtering was performed in 6.6 mbar under 50 sccm of argon flow. All sputtered films were 60 nm in thickness. Using calculated densities based on crystal structure for Pt_3Y, Pt_5Gd and Pt_5Tb, the initial platinum loadings of the gas diffusion electrodes (GDEs) were 129 $\mu g_{Pt}/cm^2$ for Pt, 99 $\mu g_{Pt}/cm^2$ for Pt_3Y, 108.4 $\mu g_{Pt}/cm^2$ for Pt_5Gd and 108.8 $\mu g_{Pt}/cm^2$ for Pt_5Tb.

2.2. MEA assembly

For all PEMFC measurements the following membrane electrode assembly (MEA) preparation was used. An 11 mm diameter circular thin-film electrode was punched from the sputtered GDL. Prior to MEA assembly the GDE were treated in 0.1 M $HClO_4$ for a total of 45 min, and rinsed with water every 15 min. This step is required to remove surface oxides of the REM alloys and creates a platinum skin on top of the alloy. To avoid the effects of hydrogen crossover in the fuel cell measurement, the model electrode was assembled with a double MEA [22]. A schematic of the double MEA configuration is shown in Fig. S10 in the supporting information. The assembly consisted of a Sigracet 25BC GDL (20 mm in diameter) at the anode side, then a commercial MEA (loading of 0.45 and 0.4 $mg_{catalyst}$ cm^{-2}) providing both the anode electrode and an interlayer of Pt catalyst. Finally, a Nafion 212 membrane was placed between the sputtered GDE and the commercial MEA, insulating the interlayer Pt from contact with the cathode GDE. Prior to any measurements, the MEA was pressed within the cell house using a clamping pressure of 12 bar at 80 °C for 30 s.

2.3. Electrochemical measurements

All measurements were performed using an in-house developed single cell with a spiral flow field [26,27]. First the cell was heated to 80 °C, with a humidifier temperature of 80 °C. To avoid condensation, the pipes between humidifier and cell were heated to 84 °C. Activation was performed by cycling between 0.9 and 0.6 V, for 2000 cycles with a sweep rate of 20 mVs^{-1} with H_2 and O_2 gas with flow rates of 14.8 ml_n min^{-1} and 29.4 ml_n min^{-1}. After this the O_2 flow was lowered to 7.4 ml_n min^{-1} and 100 cycles between 0.9 and 0.3 V were performed. Then the polarization curve was obtained by sweeping between 0.9 and 0.3 V with a sweep rate of 1 mV s^{-1} three times and taking the average of the forward sweeps. The setup was then cooled with nitrogen flow overnight. The next day the gases were switched to 5% H_2 in Ar at the anode (counter and reference electrode) and N_2 at the cathode (working electrode) in order to be able to do cyclic voltammetry (CV) and CO-stripping voltammetry in the fuel cell environment. The cyclic voltammetry was performed between 0.1 and 1.2 V, with a scan rate of 200 mV s^{-1} for 20 cycles, then with a sweep rate of 100 mV s^{-1} for 20 cycles, and finally with sweep rate of 20 mV s^{-1} for 2 cycles. Afterwards, CO-stripping was done by first recording a baseline CV between 0.1 and 1.2 V, with a scan rate of 200 mV s^{-1} for 5 cycles. This was followed by a potential hold at 0.15 V, where the gas at the cathode was switched to 2% CO in Ar for 2 min. The gas was then switched back to N_2 for 5 min purge at the same potential to ensure that all unreacted CO was removed before measuring the stripping curve in a CV as described above. The CO-stripping procedure was repeated four times. The high sweep rate of 200 mV s^{-1} was chosen to avoid excessive oxidation and degradation of the samples and to increase the measured current response. All electrochemical measurements were performed using a PAR 273A potentiostat.

2.4. Physical characterization

The X-ray photoelectron spectroscopy (XPS) (PerkinElmer PHI 5000 C ESCA system) analysis was used to study the surface composition of the four thin films (Pt, Pt_3Y, Pt_5Gd and Pt_5Tb). The surface analysis was performed using a monochromatic AlKα (1486.7 eV) X-ray source and the concentric hemispherical analyzer was positioned at a 45° angle with respect to the sample normal. Measurements with XPS were performed for as-sputtered samples, acid treated, and after electrochemical testing in the single cell fuel cell setup. For all samples, the binding energy scale was adjusted by shifting the spectra with respect to the Pt $4f_{7/2}$-peak at 71.2 eV. We notice that this choice of binding energy adjustment placed the C 1s peak around 284.4 eV on all samples.

Scanning electron microscopy (SEM) with energy-dispersive X-ray spectroscopy (EDX) was used to image and characterize the deposited catalysts. SEM was performed using a Zeiss Supra 60VP field-emission microscope at 10 kV acceleration voltage and a working distance around 4 mm. EDX was performed in the same microscope with an IXRF spectroscopy unit. The working distance of the sample was increased to 23 mm and the acceleration voltage to 20 kV during EDX.

The synchrotron radiation photoelectron spectroscopy (SRXPS) measurements were carried out at the Materials Science Beamline (MSB) at the Elettra synchrotron light source in Trieste on an ultra-high vacuum (UHV) end-station with a base pressure below 5×10^{-10} mbar. With a bending magnet source, the MSB provides synchrotron light of a high intensity in the energy range of 21 – 1000 eV. The UHV experimental chamber is equipped with a hemispherical electron energy analyzer (Specs Phoibos 150). Pt_3Y, Pt_5Gd and Pt_5Tb on GDL were measured in the SRXPS before acid treatment (as deposited), post acid treatment and after measurement in fuel cell. While conventional XPS allows for surface characterization of the samples the SRXPS measurements allow for both more accurate characterization, as well as allowing for depth probing by adjusting the photon energies.

The spectra of interest were Pt 4f, Y 3d, O 1s and C 1s acquired with photon energies of 250, 410, 650 and 990 eV . The total spectral resolutions were about 200 meV ($h\nu$ = 250 eV), 410 meV ($h\nu$ = 410 eV), 650 meV ($h\nu$ = 650 eV) and 1 eV ($h\nu$ = 990 eV).

Spectra were fitted using KolXPD software. Before fitting, each spectrum was charge corrected using the Fermi edge measured with the same photon energy. A linear background was subtracted from all data. In case of the core level Pt 4f spectra fitting procedure, the doublet separation for Pt 4f doublet components was set to 3.33 eV and the area ratio to 1.33 [18,19], the energy position of the $4f_{7/2}$ peak was constrained to be between 70 and 71 eV. The metallic component of Pt 4f was fitted using a Doniach-Šunjić line shape setting the asymmetry to 0.19 [21]. The asymmetry contribution for the adsorbed CO component was allowed to vary from 0 to 0.19 and the oxide component was fitted with a Voigt line shape with no asymmetry.

The core level Y 3d spectra were fitted with Voigt line shapes with a doublet split of 2.1 eV and area ratio of 1.5 [22]. The Lorentzian and Gaussian line widths were kept equal for all components. The metallic peak ($3d_{5/2}$) was constrained to be between 155.9 and 156.2 eV and the oxide between 158 and 158.3 eV [28–32]. Substochiometric oxide was set to vary around 157 eV. Gadolinium 4d core level spectrum is reported to be composed of a broad multiplet structure but was fitted using a single doublet with a doublet separation of 5.4 eV and doublet ratio of 1.5 for Gd $4d_{5/2}$-Gd $4d_{3/2}$ [33]. Doniach-Šunjić line shapes were used for the fitting with no asymmetry. The metallic Gd peak ($4d_{5/2}$) was set at 140.6 eV (± 0.2 eV) and the Gd_2O_3 peak at 142.8 eV (± 0.2 eV), which are consistent with previously reported Gd peaks [34–36]. Likewise, terbium 4d spectrum presents a complex multiplet structure that was fitted using singlets instead of doublets due to the lack of reliable literature for the doublet structure. It presents two different oxidation states (Tb^{3+} and Tb^{4+}) composing a mixed oxide (Tb_4O_7) [33,37,38]. Voigt line shapes with no asymmetry were used for the fitting of the three states. The metallic Tb peak ($4d_{5/2}$) was constrained at 147.5 eV, Tb^{3+} at 150.7 eV and Tb^{4+} at 154.6 eV [39,40]. All Tb peaks were allowed to vary by ± 0.2 eV.

3. Results and discussion

3.1. Electrochemical characterization

As the introduction of an alloying element should affect the structure energy of Pt skin, CV and CO-stripping were employed to electrochemically investigate the catalyst surfaces. The shape and position of the hydrogen adsorption/desorption (HAD) and the PtO redox peaks in the base CV as well as the CO-oxidation peak in CO-stripping voltammetry give information about the surface structure of the platinum [13,41–43]. The cyclic voltammetry sweeps for all PtREM samples, compared to pure platinum, are shown in Fig. 1. As can be seen the general features for all CVs are the same. This means that all alloy catalysts have pure platinum on their surfaces.

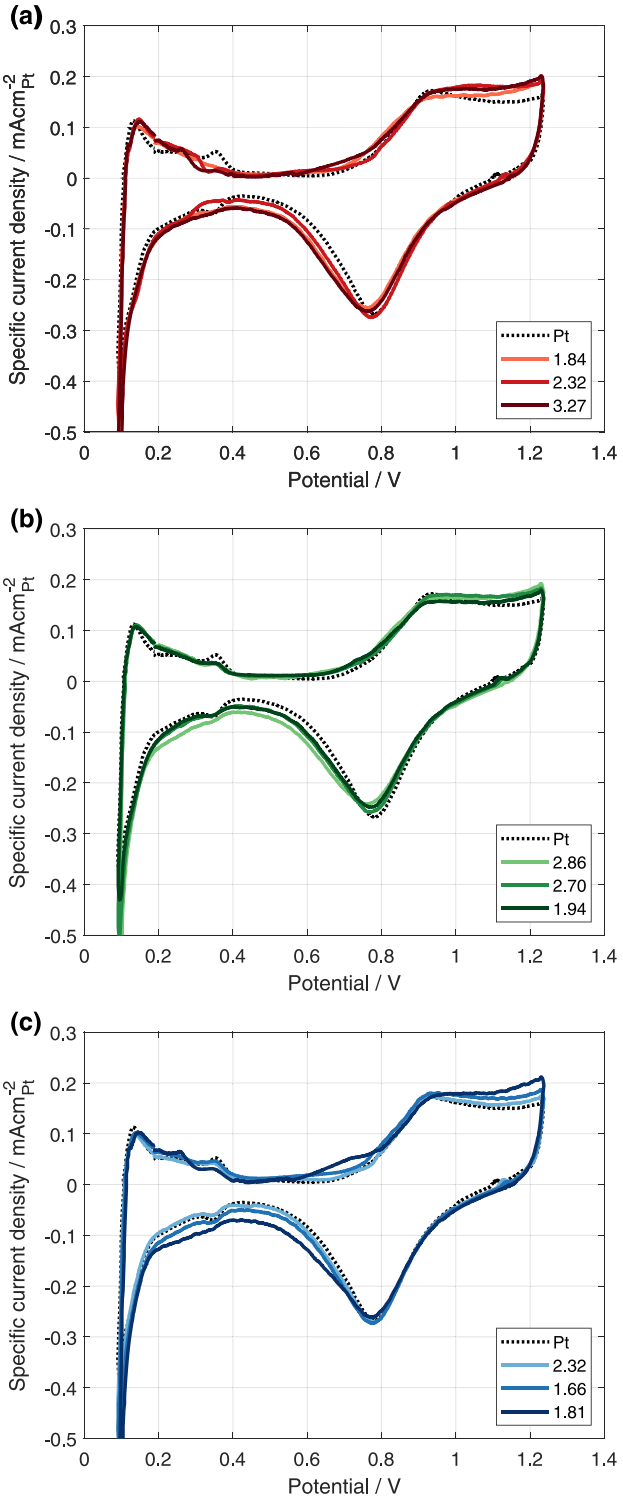

Fig. 1. Cyclic voltammetry for three repetitions of (a) Pt_3Y (b) Pt_5Gd (c) Pt_5Tb. The values in the legend are the specific activity increase at 0.9 V for each sample compared to thin-film platinum. Measured with 5% H_2 in Ar and N_2, a cell temperature of 30 °C and 100% RH, and a sweep rate of 200 mV s^{-1}.

Further, as no new peaks are visible in the alloyed samples, the REMs are not electrochemically active in the investigated potential region. Nevertheless, the alloyed catalysts have shifts in their potential responses, which indicate alterations of the surface properties compared to pure platinum. The main change that can be observed is the shift of the oxide reduction peak, which can be

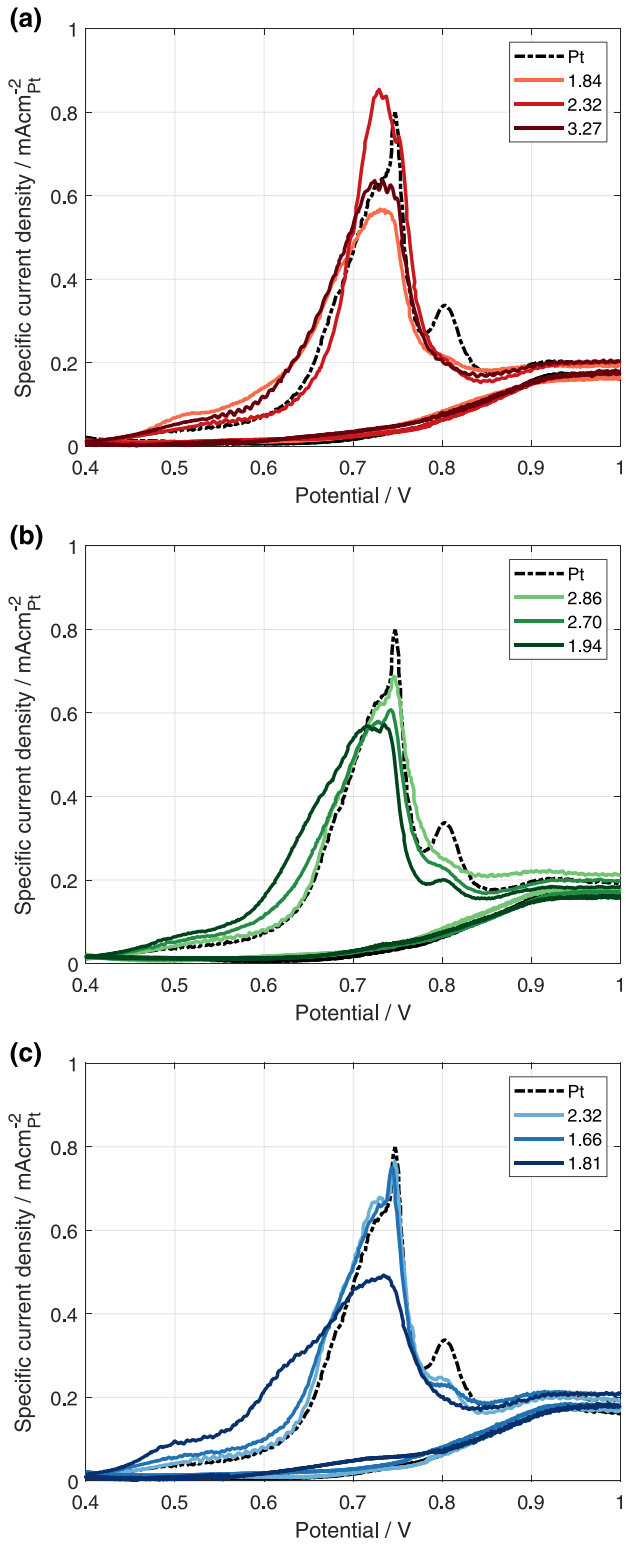

Fig. 2. CO-stripping curves for three repetitions of (a) Pt_3Y, (b) Pt_5Gd, and (c) Pt_5Tb. The values in the legend are the specific activity increase for each sample compared to thin-film platinum. Measured with 5% H_2 in Ar and N_2, a cell temperature of 30 °C and 100% RH, and a sweep rate of 200 mV s^{-1}.

seen in the negative sweep between 0.9 and 0.6 V. The CV with only the oxide region is shown in Fig. S9 in the supporting information. As the shift in oxide reduction potential is not apparently evident in CV the mean oxide reduction peak position will be used to quantify the potential shift. The mean oxide reduction peak position is defined as the potential when 50% of the oxide reduction charge has been utilized. For all alloys there is a negative shift in potential for the mean oxide reduction peak in comparison to pure Pt. For Pt_3Y and Pt_5Gd this shift is significant, on average 20 mV, while Pt_5Tb only exhibits a very slight shift of 10 mV to lower potentials.

The corresponding CO-stripping results are shown in Fig. 2. The CO-oxidation peak for the pure Pt sample is split into two with a sharp spike at 0.75 V and a small peak at 0.80 V. For the alloys the second peak at 0.80 V is much smaller or absent. In most cases there is a slight shift to lower potentials for the onset of the CO-oxidation peak, when compared to pure platinum, but the variations between samples are relatively high. This is consistent with the shift in the oxide peaks and suggests that the surface has been modified by the presence of the alloy bulk. The shift for CO is smaller than for the oxides, which is expected. For Pt_5Gd and Pt_5Tb, samples with more CO-oxidation charge at lower potentials had lower activity. This could be due to an increased number of surface defects for these samples, which might explain the lower oxygen reduction activity [43].

The polarization curves for three samples of the Pt_3Y and Pt_5Gd, and Pt_5Tb thin film alloys are shown in Fig. 3. To ensure proper alloy composition the sputtered films were intentionally made flat and thick. This results in low electrochemical active surface area per mass platinum, and subsequently poor platinum utilization. As such these electrodes give a good model system for studying catalytic activity in a fuel cell, but are not optimal electrodes for an operating fuel cell. As the main focus of the study is primarily the kinetic activity of the catalyst in a fuel cell, all results will be reported in specific current density based on the measured Pt electrochemical surface area from the CO-stripping measurements, as shown in Fig. 2. Polarization curves of geometric surface area and mass activity are shown in Figs. S6 and S7 in the supporting information. CO-stripping was chosen to measure the electrochemical surface area (ECSA) due to hydrogen adsorption/desorption (HAD) often underestimates the ECSA, especially when measuring alloy catalysts and MEAs [13,42]. For all the investigated samples the ECSA obtained from HAD was approximately 50% lower than that obtained from CO-stripping.

As can be seen, the specific activity for all alloys is higher than that of pure platinum. The activity increases, shown in Table 1, are approximately 2.5 times higher for Pt_3Y and Pt_5Gd, and about 2 times higher for Pt_5Tb. The lower activity for Pt_5Tb, compared to Pt_3Y and Pt_5Gd, could be due to the lower stability of Pt_5Tb [2]. While the stabilities of the alloy catalysts have not been specifically measured, it should be noted that all samples have been cycling between 0.9 and 0.6 V for ~16 h before the activity measurement. As seen in Table 1, the activity increase at 0.75 V is lower than at 0.9 V. This is most likely due to other effects, such as local mass transport, affecting the measurement. Nevertheless, all the alloys show higher activity, at 0.75 V, with improvements of 1.7 for Pt_3Y, 1.5 for Pt_5Gd and 1.6 for Pt_5Tb. The previously reported activity for Pt/C nanoparticles is approximately 200 μA cm^{-2}_{Pt} [44]. The sputtered films of pure platinum have a higher activity of 280 μA $cm^{-2}_{Pt,}$ compared to nanoparticles, which was also observed in RDE measurements [15]. This is attributed to strains in the platinum films from substrate interactions [45]. Comparing the measured alloys to the activity of platinum nanoparticles gives improvement factors of 3.5 for Pt_3Y and Pt_5Gd, and 2.7 for Pt_5Tb. The mass activities, at 0.9 V, of the sputtered electrodes are 0.011 (Pt), 0.026 (Pt_3Y), 0.028 (Pt_5Gd) and 0.018 A/mg_{Pt} (Pt_5Tb). The low values compared to 0.15 A/mg_{Pt} for Pt/C electrodes [11] is due to that the sputtered 60 nm catalyst has a much lower surface to volume ratio compared to nanoparticle catalysts. Even so, the corresponding mass-activity increase of the alloyed films at 0.9 V is significant, compared to the platinum film, being a factor of 2.8 (Pt_3Y), 1.7 (Pt_5Gd), and 2.2 (Pt_5Tb).

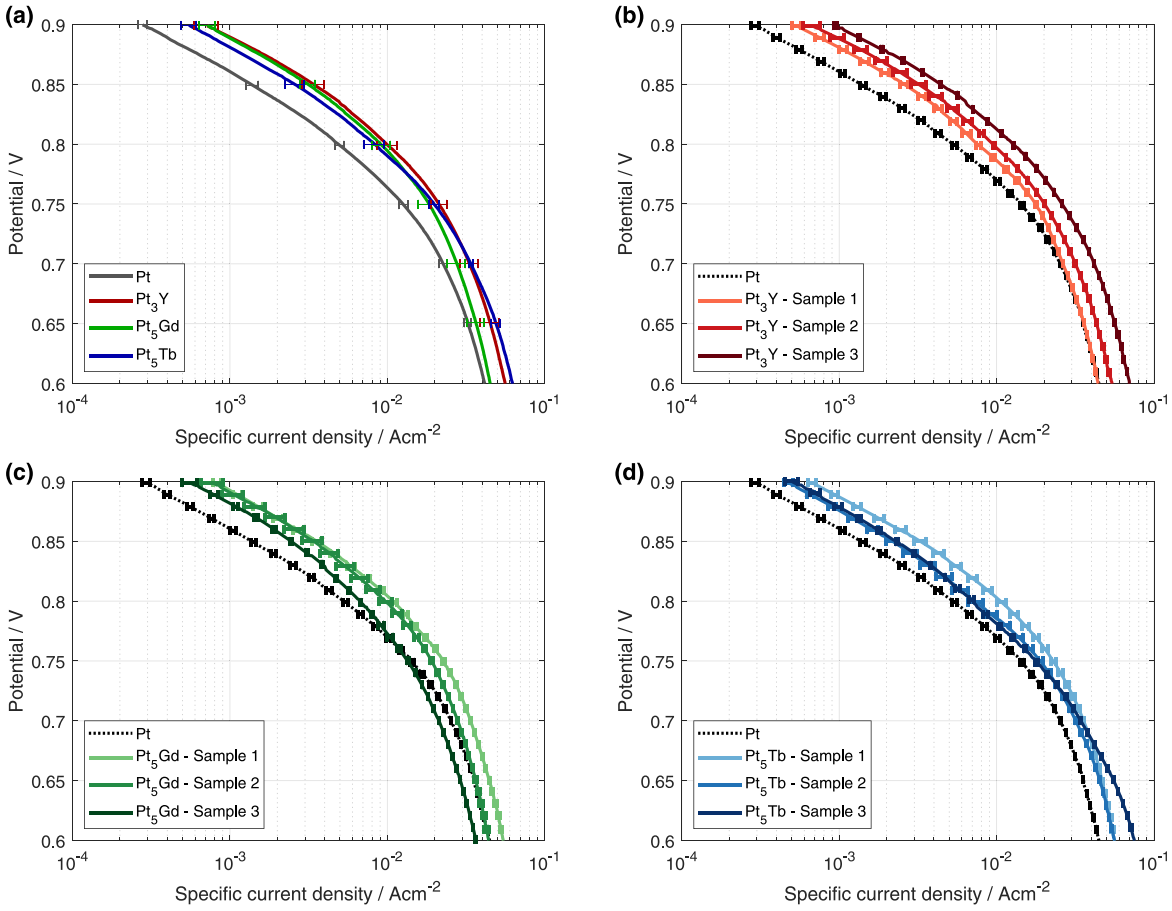

Fig. 3. Specific activity of the different tested alloy catalysts, (a) Mean value for all measurements. Error bars show the standard error for each alloy. (b–d) Specific activity for three repetitions of (b) Pt_3Y (c) Pt_5Gd (d) Pt_5Tb. Measured with 14.8 ml_n min^{-1} H_2 and 7.4 ml_n min^{-1} O_2, a cell temperature of 80 °C, 100% RH, and a sweep rate of 1 mV s^{-1}. The electrochemical surface area was calculated from CO-stripping. The error bars represent the standard deviation of the three forward sweeps.

Table 1
Mean specific current density, at 0.9 and 0.75 V, and standard deviation between repeated experiments for different samples. The improvement factor is compared to sputtered platinum and calculated from the specific activity at 0.9 V.

Sample	$i_{0.9\ V}$ μA $cm^{-2}{}_{Pt}$	$i_{0.75\ V}$ mA $cm^{-2}{}_{Pt}$	Improvement factor compared to thin film Pt
Pt	280 ± 30	12.6 ± 1.5	–
Pt_3Y	692 ± 200	21.3 ± 4.3	2.48 ± 0.78
Pt_5Gd	699 ± 140	18.4 ± 4.6	2.50 ± 0.56
Pt_5Tb	539 ± 100	19.8 ± 2.6	1.93 ± 0.41

Considering the large variation of activity between samples, the activity increase as a function of mean oxide peak position and ECSA were investigated more closely. When comparing the mean oxide reduction peak position, calculated from the reduction charge from Fig. 1, with activity it can be seen that the more active samples exhibit a peak position at slightly lower potentials, as shown in Fig. 4a. However, a shift to lower potentials would indicate an increase in binding energy, not the expected decrease [2,3,25]. The shifts detected here are most likely due to the presence of several crystal planes of platinum. Exactly what is causing the negative shift in peak position is still unclear, but the shift has been reported previously for sputtered PtREM catalysts [14,15,46,47]. Fig. 4b shows the activity increase as a function of the ECSA. The cause of the large in-sample variance of ECSA for the PtREM samples is at present not fully understood. Possible explanations could be variations of the MPL causing changes in the sputtered layers. The results indicate a trend that the lower the ECSA, the higher the measured activity. Previous studies have shown that sputter deposition onto an MPL creates particles with varying size, with regions that are less than 3 nm [16]. These thin regions fully leach out the REM during acid treatment, and become pure platinum. As such, a high ECSA could indicate that the sample has more of these pure platinum regions, which lowers the overall activity of the sample. Further, the ECSA value is an indication of the surface roughness of the samples, meaning that a low ECSA indicates flatter surface. This result suggests that if the surface becomes too rough, the macrostrain caused by the alloy become less significant, lowering the expected activity increase. A rougher surface could indicate that the surface has more disordered platinum, which is less active compared to the ordered structure [43,48].

The electrochemical results show that the presence of an alloying element affects the electrochemical properties of platinum, which results in higher intrinsic activity. The shifts in potential can be seen in the CVs and CO-stripping measurements, however, due to the polycrystalline nature of the sputtered films, the exact cause of the shifts is difficult to quantify.

3.2. Physical characterization

The samples were physically characterized by energy-dispersive X-ray spectroscopy (EDX), which has a sensing depth in the micrometer range and, thus, gives information about the bulk composition of the sputtered films. Fig. 5a shows the Pt:REM bulk com-

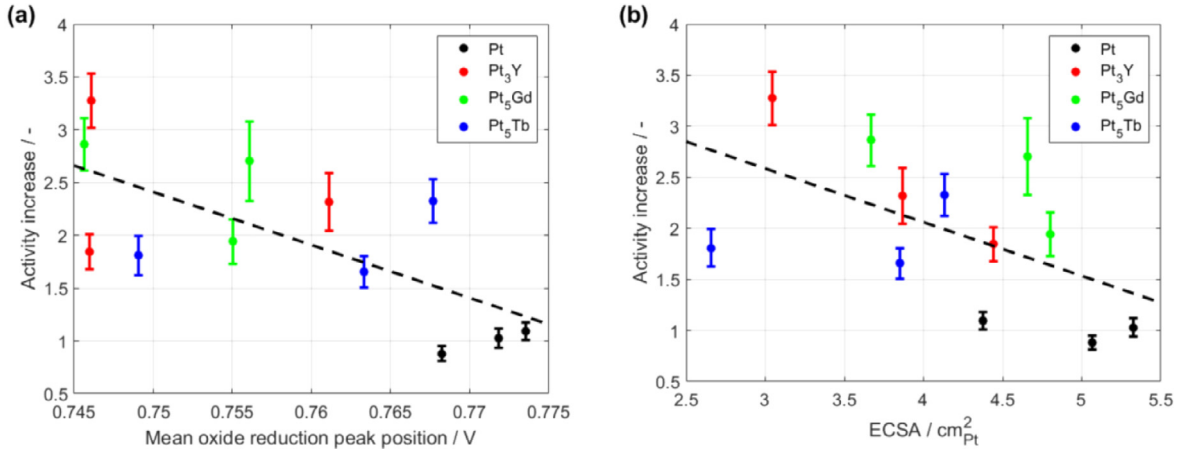

Fig. 4. Activity increase as a function of mean oxide reduction peak position (a) and the electrochemical active surface area (b). Measured with 5% H_2 in Ar and N_2, a cell temperature of 30 °C and 100% RH, and a sweep rate of 200 mV s^{-1}. Trend line is for visual aid only.

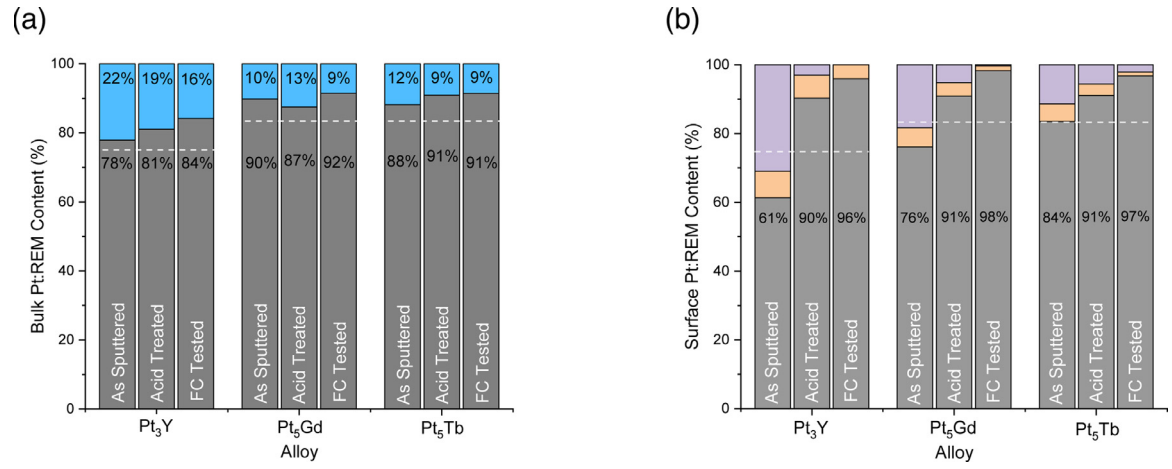

Fig. 5. (a) The bulk content of Pt:REM for each sample measured by EDX. Gray colored columns indicate Pt and blue the REM of each alloy. (b) The surface content of Pt:REM for each sample measured by XPS. Gray corresponds to Pt, orange metallic REM and purple REM-oxide. Numeric percentages of each alloy are found in Table S2 in Supporting Information. Dashed white lines indicate the composition of the sputter target for the different alloys.

position ratio of the three different alloys as sputtered, after acid treatment, and after electrochemical test. The EDX analysis confirms that the bulk nominal composition obtained is very close to that of the sputter target alloys with the ratios 3:1 (Pt_3Y) and 5:1 (Pt_5Gd and Pt_5Tb). The spread in REM content after acid treatment and fuel cell operation, falls into the EDX error margin expected for samples supported onto porous surfaces [49]. Therefore, it appears that all alloys maintain their bulk composition after acid treatment and fuel cell operation, indicating that the bulk alloy is mostly unchanged and the platinum overlayer, which forms after acid treatment, is so thin that it does not affect the bulk composition.

The samples were also characterized by X-ray photoelectron spectroscopy (XPS), which has a probing depth of a few nanometers, meaning only the surface elemental composition of these films is determined. The XPS results for all tested alloys are shown in Fig. 5b. The as-sputtered samples all showed a much larger Pt:REM surface relative amount than given by nominal ratios, which is also considerably larger than the ratio measured in EDX, thereby suggesting that there is a surface enrichment of REM during sputtering. During acid treatment the surface REMs that oxidized, due to contact with air, were removed. This is the cause for the large reduction of REM seen in the XPS, more pronounced than in EDX. After the electrochemical tests, all alloys show a decrease in their total surface REM content to only between 5 and 7% remaining close to the surface. This can be attributed to the further leaching of the alloy and an increase in overlayer thickness as a result of the exposure to the acidic fuel cell environment and the electrochemical reactions taking place during fuel cell evaluation [15,22].

To present the oxide and metallic REM XPS data in more detail, the fitted spectra for the REM components Y 3d (Pt_3Y), Gd 4d (Pt_5Gd) and Tb 4d (Pt_5Tb), as sputtered, after acid treatment, and after fuel cell measurements are shown in Fig. 6. For all alloys, similar trends can be observed. The as-sputtered samples all have peaks corresponding mainly to the non-metallic state of the REM. The non-metallic peaks in the as-sputtered samples are attributed to the formation of oxides as a result of exposure to ambient atmosphere after sputter deposition [17]. After acid treatment, the amount of REM to platinum decreases as oxidized REM is removed from the surface resulting in a significant reduction in intensity of the Y 3d, Gd 4d, and Tb 4d core level peaks. Before treatment, all REM in contact with the air is oxidized so the surface contains mostly REM-oxide and some metallic REM in the layers below. Acid treatment removes the REM-oxides, leaving only metallic REM in the bulk material. Thus, a layer of platinum is formed where the REM-oxides were leached. This is also in accordance with previous results, showing the formation of a protective Pt overlayer when PtREM samples are immersed in an acidic solution [2,25,46]. The REM peaks in the XPS spectra of Pt_5Gd and Pt_5Tb are reduced in amplitude as they contain much less REM than Pt_3Y. Additionally,

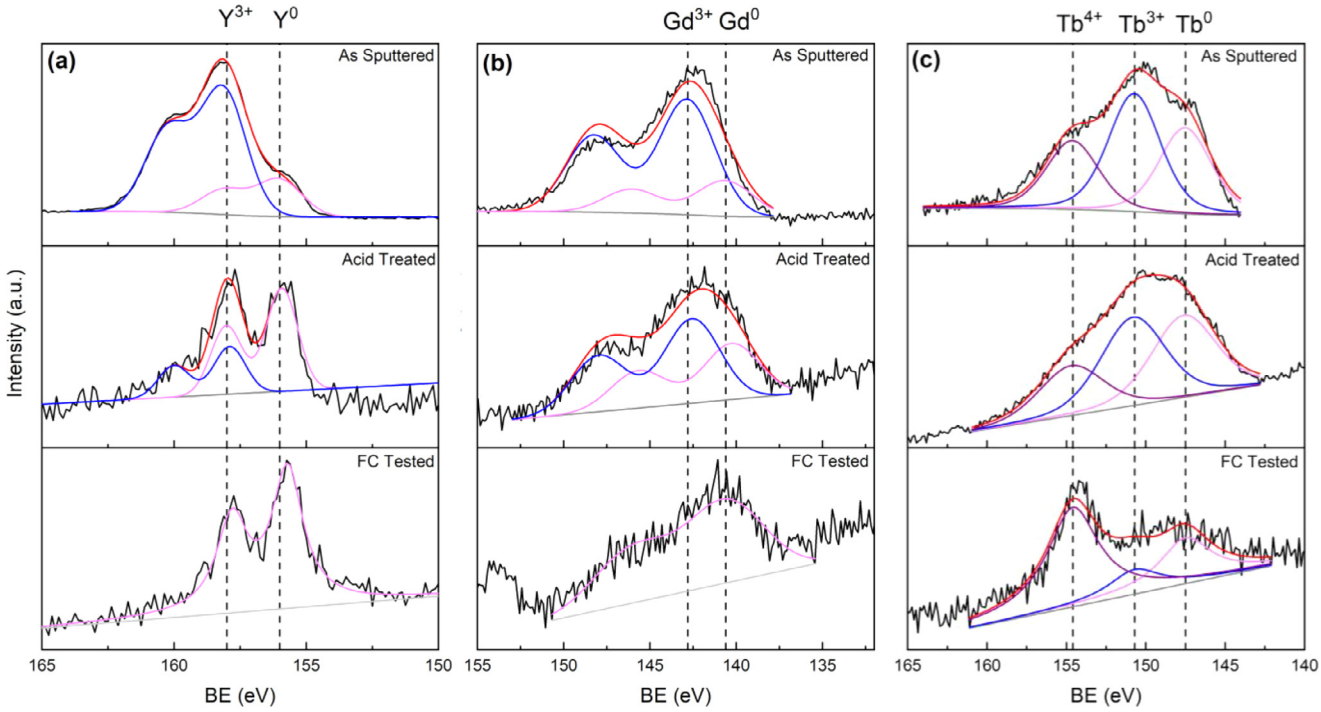

Fig. 6. XPS spectra of (a) Y 3d (Pt_3Y) (b) Gd 4d (Pt_5Gd) and (c) Tb 4d (Pt_5Tb) for as sputtered, acid cleaned and post electrochemical measurements. All 3d orbitals shown correspond to $3d_{5/2}$ orbitals. The red line corresponds to the fitted spectrum, pink the metallic REM and blue and purple the REM oxide (For interpretation of the references to color in this figure legend, the reader is referred to the web version of this article).

the XPS cross-sections for Tb and Gd are also lower than Y which further decreases signal making quantitative analysis of the peak constituents difficult to perform. The amount of oxides remaining after acid treatment seems to be higher for Pt_5Gd and Pt_5Tb, compared to Pt_3Y, which can be attributed to either subsurface REM-oxides present also after acid treatment or some REM–O coordination in the thin film surface [14,50].

After fuel cell operation, the amount of REM-oxide decreases for all samples. This result suggests that the electrochemical measurements cause additional leaching from beneath the surface. There were no significant changes observed in the Y 3d and Gd 4d peaks for Pt_3Y and Pt_5Gd, only a slight reduction in the total amount of REM near the surface. For Pt_5Tb, a slight decrease in the total and metallic amount of Tb is observed. The relatively low amount of metallic Tb observed in XPS, compared to the others, might explain the somewhat lower fuel cell performance of this alloy. The differences between the XPS data after acid treatment and electrochemical measurements suggest that the alloys are affected differently by the fuel cell environment. As such, there might be different optimal activation strategies for each type of alloy, which can lead to higher ORR activities.

In general, the overlayer thickness increases after fuel cell use as the total amount of REM decreases for all alloys. Films sputtered on a porous and particulate GDL are not flat and have thickness variation, this is shown in Figs. S4 and S5 in the supporting information, so some areas of the sputtered films are thin and allow complete oxidation of the REM [22]. Regions under 3 nm in thickness are less active, as the REM leaches from the bulk to become pure Pt after acid treatment [15]. Fuel cell operation causes further leaching and an increase in the areas of pure Pt. Hence, catalyst layers sputtered onto GDL have lower increases in activity, compared to the RDE measurements of the same alloys on flat glassy carbon substrates [15].

Synchrotron radiation can provide a depth profile of the surface composition through changing beam energy and can reveal surface impurities. In a synchrotron, lower photon energies than in lab-XPS are used to reduce the depth probed and gain more surface sensitivity. In general, Tb and Gd produce less signal than Y as they have lower photoionization cross-sections, so it is harder to measure them with low photon energies provided by a synchrotron, especially in the low alloy concentrations used in this study. Therefore, it was only possible to measure Pt_3Y in this manner. Measurements of the Y 3d core level peak in Pt_3Y samples are presented in Fig. 7.

Before acid treatment, all yttrium at the surface is oxidized, as indicated by the two oxide doublets present in the Y 3d core level in Fig. 7a, that are seen at higher energy compared to metallic yttrium. Pure yttrium oxide is the doublet at 158.3 eV and a substochiometric oxide is the doublet at 157.5 eV. As photon energy is increased there is more contribution from metallic yttrium as the relative amount of substochiometric oxide is reduced. Notably there is still a large contribution from yttrium oxide even at 990 eV corresponding to a depth of approximately 2.4 nm.

The acid treatment in 0.1 M $HClO_4$ removes most of the yttrium from the surface, shown in Fig. 7b, as higher photon energies show only metallic yttrium remains due to the yttrium oxide being leached out. This confirms the formation of the platinum overlayer. Our previous work studying flat sputtered Pt_3Y in the synchrotron showed more yttrium underneath the surface compared to the porous GDL substrates in this study [32]. This is due to the GDL structure, where Pt_3Y will also be sputtered around the edges of the carbon particles [15]. Acid treatment removes more yttrium on a GDL substrate compared to a flat substrate, as described above alongside lab-XPS [32]. Subsequent fuel cell exposure appears to remove a little more yttrium, nevertheless, the surface is mostly unchanged by the electrochemical testing and no additional surface impurities were observed.

Comparing the content of the surface for each photon energy reveals features of the catalyst layer on the GDL. Fig. 8 summarizes the results of the fitting of the spectra showing the relative

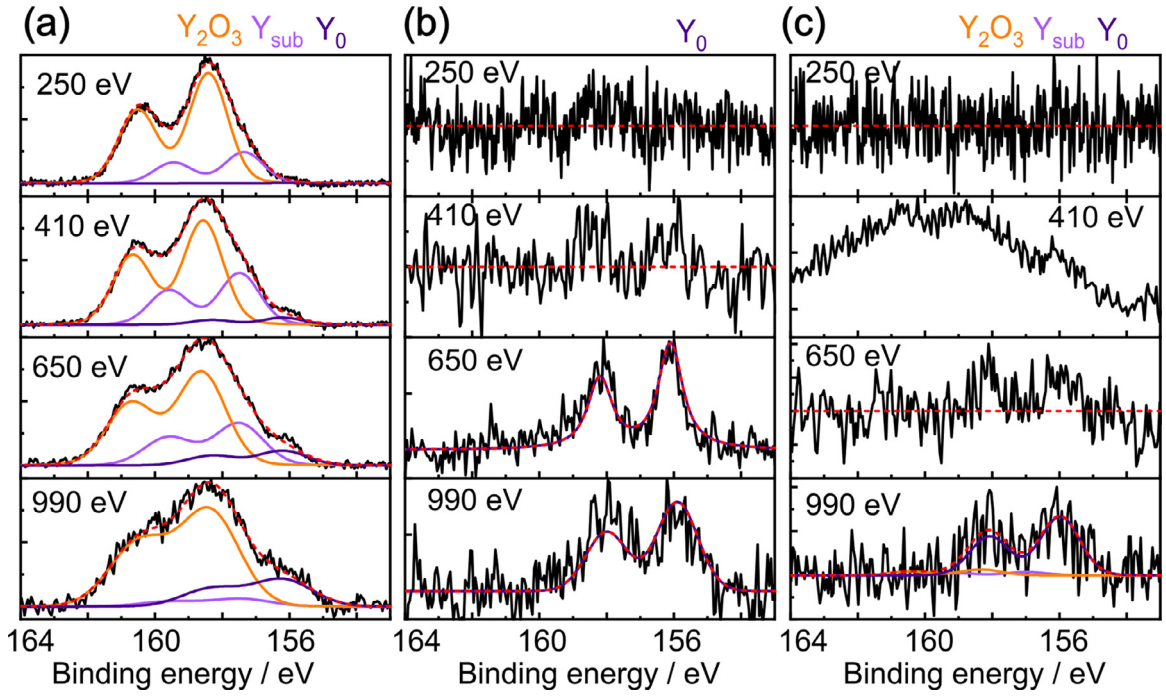

Fig. 7. The catalyst surface seen through the Y 3d core level; (a) as sputtered Pt_3Y, (b) acid treated and (c) post-fuel cell test. Yttrium oxide (orange), substochiometric oxide (light purple) and metallic yttrium (dark purple) are present in the as-deposited sample. Only metallic yttrium (dark purple) is present in the acid treated and fuel cell tested samples (For interpretation of the references to color in this figure legend, the reader is referred to the web version of this article).

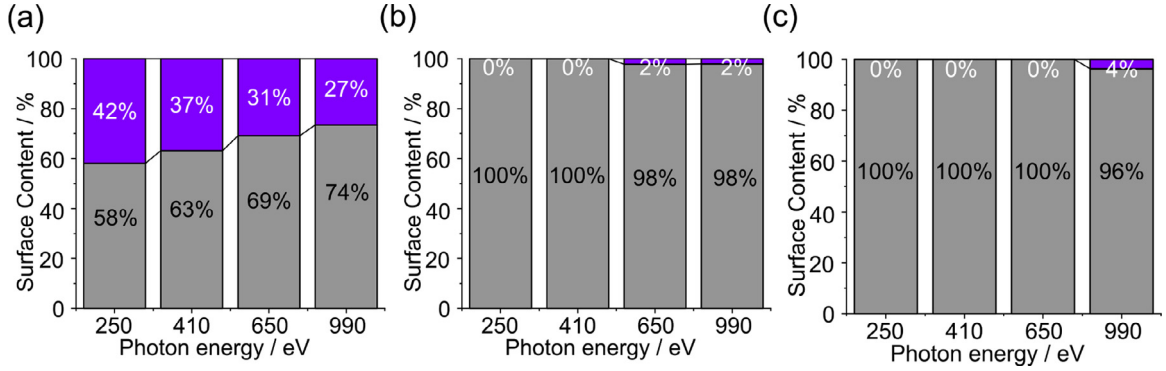

Fig. 8. The percentage content of Pt 4f (gray) and Y 3d (purple) for (a) as-deposited, (b) acid treated and (c) post-fuel cell test at each photon energy (For interpretation of the references to color in this figure legend, the reader is referred to the web version of this article).

amount of Pt 4f and Y 3d corrected using the spectrometer transmission and elemental cross-section. There is an enrichment of surface REM and REM-oxides in the as-deposited sample, in agreement with the conventional XPS results presented in Fig. 5b. At 990 eV the stoichiometry of the alloy is as expected. There is little difference between the amount of Pt:Y in the acid treated and fuel cell tested sample. On first glance it seems that there is slightly less yttrium in the fuel cell tested sample, observed by no REM being detected at 650 eV. However, due to the large noise and error in fitting it can be concluded that both samples have a very similar surface. Fuel cell tests conducted in the manner presented in this paper do not alter the catalyst surface significantly.

The as prepared GDL supported Pt, Pt_3Y, Pt_5Gd and Pt_5Tb thin films were structurally characterized by XRD and shown in Fig. S11. The pure Pt film clearly show visible diffraction peaks of Pt(111) ,(200) and (220), characteristic of an FCC crystal structure [51,52], and confirms the presence of a crystalline Pt film. However, the characteristic peaks for the 60 nm Pt film are relatively weak in comparison to bulk Pt. Further, the carbon GDL used as a substrate gives rise to an intense and broad diffraction peak at 25° and a large background in all samples. In comparison to Pt, the PtREM samples show very small and broad peaks associated with the Pt diffraction and no new peaks for other crystalline structures, pointing towards the formation of alloys of smaller grain sizes and a more amorphous character. The diffuse diffraction makes it difficult to deduce the presence of a lattice strain from these measurements.

The presented results show that the specific activity for sputtered thin-film PtREM catalysts is superior to that of a thin film of pure Pt. The electrochemical and physical characterization both show that an overlayer has been formed, and that it remains after electrochemical testing. Further, after testing additional leaching of REM is minor. This leaching is most likely occurring in areas of the MPL where the deposited film is thinner and results in areas of pure Pt, which may be one of the explanations to the lower activities observed in the fuel cell compared to RDE. This is supported by the depth profiles in Fig. 8, where no increase in overlayer thickness was observed. Further, the electrochemical mea-

surements do not cause a significant change in the Pt_3Y, which has a nearly constant composition before and after the electrochemical testing. This suggests this alloy is stable in the operating range of a fuel cell. This is further supported by the SEM images, Fig. S5 in supporting information, where no significant changes in morphology is observed after electrochemical testing. The effect of acid treatment and electrochemical evaluation in the fuel cell on the Pt_3Y surface properties was evaluated in detail by transmission electron microscopy (TEM) in our previous paper [22]. We expect that the other alloys have a similar behavior as Pt_3Y in that case. A more in-depth evaluation of the surface changes of Pt_3Y films during long-term fuel cell measurements including TEM and SRXPS is currently being carried out. Pt_5Gd shows similar trends as Pt_3Y with a similar amount of metallic REM before and after electrochemical testing. The lower measured activity of Pt_5Tb is most likely due to leaching of the REM, which causes a thicker, and subsequently less strained, Pt overlayer. Further studies are required to fully determine the stability of these materials. The large variation between samples as well as the similar values between the investigated PtREM alloys suggests that the uneven substrate and the presence of undefined areas with no REM content are significantly affecting the catalyst activity. If these regions could be removed, even higher activities should be obtainable. Nevertheless, all evaluated alloy samples have higher activity compared to pure platinum, indicating that PtREM alloy catalysts can achieve high activity in an active fuel cell.

4. Conclusion

In this work the activity of sputtered thin films of Pt_3Y, Pt_5Gd and Pt_5Tb in a PEMFC were evaluated. It was found that the specific activity of Pt_3Y and Pt_5Gd were approximately 2.5 times that of pure platinum. The slightly lower activity enhancement of Pt_5Tb, approximately 2 times that of pure platinum, was due to lower amounts of metallic REM found after the electrochemical tests, most likely due to the formation of a thicker platinum layer. This suggests that Pt_5Tb is less stable than Pt_5Gd and Pt_3Y in PEMFC environment. Cyclic voltammetry and CO-stripping curves showed small potential shifts to higher binding energies for the oxide peaks. This is attributed to changes in the bulk composition of the alloys, caused by the introduction of the alloying element. XPS and EDX measurements showed that acid treatment removes surface REM-oxides. However, after electrochemical tests all alloys had different amounts of REM as well as different ratios between metallic and oxidized REM, suggesting that there might be different optimal activation strategies for the different alloys. If these strategies can be found, even higher activities could be achieved. Pt_3Y showed no significant change in the surface composition, suggesting that this alloy is the most stable under the experimental conditions. The high activity, combined with the low changes in surface composition, achieved in an operating fuel cell shows that PtREM catalysts are promising as ORR catalysts in PEMFC.

5. Creadit author statement

B.E., R.W.L., G.L. and C.L. designed the electrochemical experiments. B.E. performed the single cell fuel cell measurements and electrochemical characterization. R.B. performed the sputter deposition of the PtREM samples and G.M.S. performed the XPS analysis. R.B., G.M.S. and T.S performed the SRXPS measurements. R. B. and G.M.S. performed the SEM and EDX analysis. B.E. and G.M.S. wrote and edited the paper with the input from all authors. All authors discussed the results, read and approved the final version of the paper.

Declaration of Competing Interest

The authors declare that they have no known competing financial interests or personal relationships that could have appeared to influence the work reported in this paper.

Acknowledgments

This work was supported by the Strategic Vehicle Research and Innovation program (FFI) (Project No. P37806–3), the Swedish Foundation for Strategic Research (SSF) (Project No. EM16–0060), the Swedish governmental initiative StandUp for Energy and the Swedish Research Council (Project No. 2018–03927). Sample fabrication was performed in part at Myfab, Chalmers. Dr. Niklas Lindahl is acknowledged for the initial sputter deposition of the PtREM samples. We thank CERIC-ERIC for access to the synchrotron facilities and for financial support. We also thank Chalmers Materials Analysis Laboratory (CMAL) for performing the XRD measurements.

Supplementary materials

Supplementary material associated with this article can be found, in the online version, at doi:10.1016/j.electacta.2021.138454.

References

[1] J. Marcinkoski, J. Spendelow, A. Wilson, D. Papageorgopoulos, P. Reviewed, R. Ahluwalia, B. James, C. Houchins, J. Moton, Fuel cell system cost -2015, DOE Hydrog, Fuel Cell. Progr. Rec. Rec (2015) 15015, https://www.hydrogen.energy.gov/pdfs/15015_fuel_cell_system_cost_2015.pdf.

[2] M. Escudero-Escribano, P. Malacrida, H.M. Hansen, U. Vej-Hansen, A. Velazquez-Palenzuela, V. Tripkovic, J. Schiøtz, J. Rossmeisl, I.E.L. Stephens, I. Chorkendorff, Tuning the activity of Pt alloy electrocatalysts by means of the lanthanide contraction, Science 352 (80) (2016) 73–76.

[3] J. Greeley, I.E.L. Stephens, a S. Bondarenko, T.P. Johansson, H. a Hansen, T.F. Jaramillo, J. Rossmeisl, I. Chorkendorff, J.K. Nørskov, Alloys of platinum and early transition metals as oxygen reduction electrocatalysts, Nat. Chem. 1 (2009) 552–556, doi:10.1038/nchem.367.

[4] R. Sakamoto, K. Omichi, T. Furuta, M. Ichikawa, Effect of high oxygen reduction reaction activity of octahedral PtNi nanoparticle electrocatalysts on proton exchange membrane fuel cell performance, J. Power Sour. 269 (2014) 117–123, doi:10.1016/j.jpowsour.2014.07.011.

[5] C. Chen, Y. Kang, Z. Huo, Z. Zhu, W. Huang, H.L. Xin, J.D. Snyder, D. Li, J.A. Herron, M. Mavrikakis, M. Chi, K.L. More, Y. Li, N.M. Markovic, G.A. Somorjai, P. Yang, V.R. Stamenkovic, Highly crystalline multimetallic nanoframes with three-dimensional electrocatalytic surfaces, Science 343 (80–) (2014) 1339–1343, doi:10.1126/science.1249061.

[6] M. Li, Z. Zhao, T. Cheng, A. Fortunelli, C.Y. Chen, R. Yu, Q. Zhang, L. Gu, B.V. Merinov, Z. Lin, E. Zhu, T. Yu, Q. Jia, J. Guo, L. Zhang, W.A. Goddard, Y. Huang, X. Duan, Ultrafine jagged platinum nanowires enable ultrahigh mass activity for the oxygen reduction reaction, Science 354 (80–) (2016) 1414–1419, doi:10.1126/science.aaf9050.

[7] D. Van Der Vliet, C. Wang, M. Debe, R. Atanasoski, N.M. Markovic, V.R. Stamenkovic, Platinum-alloy nanostructured thin film catalysts for the oxygen reduction reaction, Electrochim. Acta 56 (2011) 8695–8699, doi:10.1016/j.electacta.2011.07.063.

[8] H. Yano, I. Arima, M. Watanabe, A. Iiyama, H. Uchida, Oxygen reduction activity and durability of ordered and disordered Pt 3 Co alloy nanoparticle catalysts at practical temperatures of polymer electrolyte fuel cells, J. Electrochem. Soc. 164 (2017) F966–F972, doi:10.1149/2.1141709jes.

[9] D. Wang, H.L. Xin, R. Hovden, H. Wang, Y. Yu, D.A. Muller, F.J. Disalvo, H.D. Abruña, Structurally ordered intermetallic platinum-cobalt core-shell nanoparticles with enhanced activity and stability as oxygen reduction electrocatalysts, Nat. Mater. 12 (2013) 81–87, doi:10.1038/nmat3458.

[10] L. Zhang, X. Wang, H. Zhu, Surface modifications of Pt-based atomically ordered nanoparticles to improve catalytic performances for oxygen reduction reaction, Prog. Nat. Sci. Mater. Int. 30 (2020) 890–895, doi:10.1016/j.pnsc.2020.10.013.

[11] A. Kongkanand, M.F. Mathias, The priority and challenge of high-power performance of low-platinum proton-exchange membrane fuel cells, J. Phys. Chem. Lett. 7 (2016) 1127–1137, doi:10.1021/acs.jpclett.6b00216.

[12] K.J.J. Mayrhofer, K. Hartl, V. Juhart, M. Arenz, Degradation of carbon-supported Pt bimetallic nanoparticles by surface segregation, J. Am. Chem. Soc. 131 (2009) 16348–16349, doi:10.1021/ja9074216.

[13] T.R. Garrick, T.E. Moylan, M.K. Carpenter, A. Kongkanand, Electrochemically active surface area measurement of Aged Pt alloy catalysts in PEM fuel cells by CO stripping, J. Electrochem. Soc. 164 (2017) F55–F59, doi:10.1149/2.0381702jes.

[14] E. Zamburlini, K.D. Jensen, I.E.L. Stephens, I. Chorkendorff, M. Escudero-Escribano, Benchmarking Pt and Pt-lanthanide sputtered thin films for oxygen electroreduction: fabrication and rotating disk electrode measurements, Electrochim. Acta 247 (2017) 708–721, doi:10.1016/j.electacta.2017.06.146.
[15] N. Lindahl, E. Zamburlini, L. Feng, H. Grönbeck, M. Escudero-Escribano, I.E.L. Stephens, I. Chorkendorff, C. Langhammer, B. Wickman, High specific and mass activity for the oxygen reduction reaction for thin film catalysts of sputtered Pt3Y, Adv. Mater. Interface 4 (2017) 1–9, doi:10.1002/admi.201700311.
[16] R. Sandström, E. Gracia-Espino, G. Hu, A. Shchukarev, J. Ma, T. Wågberg, Yttria stabilized and surface activated platinum (PtxYOy) nanoparticles through rapid microwave assisted synthesis for oxygen reduction reaction, Nano Energy 46 (2018) 141–149, doi:10.1016/j.nanoen.2018.01.038.
[17] F. Masini, P. Hernández-Fernández, D. Deiana, C.E. Strebel, D.N. McCarthy, A. Bodin, P. Malacrida, I. Stephens, I. Chorkendorff, Exploring the phase space of time of flight mass selected Pt $_x$ Y nanoparticles, Phys. Chem. Chem. Phys. 16 (2014) 26506–26513, doi:10.1039/C4CP02144D.
[18] P. Hernandez-Fernandez, F. Masini, D.N. McCarthy, C.E. Strebel, D. Friebel, D. Deiana, P. Malacrida, A. Nierhoff, A. Bodin, A.M. Wise, J.H. Nielsen, T.W. Hansen, A. Nilsson, I.E.L. Stephens, I. Chorkendorff, Mass-selected nanoparticles of PtxY as model catalysts for oxygen electroreduction, Nat. Chem. (2014) 1–23, doi:10.1038/nchem.2001.
[19] R. Brandiele, A. Guadagnini, L. Girardi, G. Dražić, M.C. Dalconi, G.A. Rizzi, V. Amendola, C. Durante, Climbing the oxygen reduction reaction volcano plot with laser ablation synthesis of Pt: xY nanoalloys, Catal. Sci. Technol. 10 (2020) 4503–4508, doi:10.1039/d0cy00983k.
[20] R. Brandiele, C. Durante, E. Gradzka, G.A. Rizzi, J. Zheng, D. Badocco, P. Centomo, P. Pastore, G. Granozzi, A. Gennaro, One step forward to a scalable synthesis of platinum-yttrium alloy nanoparticles on mesoporous carbon for the oxygen reduction reaction, J. Mater. Chem. A 4 (2016) 12232–12240, doi:10.1039/c6ta04498k.
[21] Y. Hu, J. Oluf Jensen, L. Nilausen Cleemann, B. Axel Brandes, Q. Li, Synthesis of Pt–rare earth metal nanoalloys, J. Am. Chem. Soc. 142 (2019) 953–961, doi:10.1021/jacs.9b10813.
[22] N. Lindahl, B. Eriksson, H. Grönbeck, R. Wreland Lindström, G. Lindbergh, C. Lagergren, B. Wickman, Fuel cell measurements with cathode catalysts of sputtered Pt3Y thin films, ChemSusChem 11 (2018) 1438–1445, doi:10.1002/cssc.201800023.
[23] J.N. Schwämmlein, G.S. Harzer, P. Pfändner, A. Blankenship, H.A. El-Sayed, H.A. Gasteiger, Activity and stability of carbon supported PtxY alloys for the ORR determined by RDE and single-cell PEMFC measurements, J. Electrochem. Soc. 165 (2018) J3173–J3185, doi:10.1149/2.0221815jes.
[24] S.J. Yoo, K.-S. Lee, S.J. Hwang, Y.-H. Cho, S.-K. Kim, J.W. Yun, Y.-E. Sung, T.-H. Lim, Pt3Y electrocatalyst for oxygen reduction reaction in proton exchange membrane fuel cells, Int. J. Hydrogen Energy. 37 (2012) 9758–9765, doi:10.1016/j.ijhydene.2012.03.089.
[25] M. Escudero-Escribano, A.F. Pedersen, E.T. Ulrikkeholm, K.D. Jensen, M.H. Hansen, J. Rossmeisl, I.E.L. Stephens, I. Chorkendorff, Active-phase formation and stability of Gd/Pt(111) electrocatalysts for oxygen reduction: an *in situ* grazing incidence X-Ray diffraction study, Chem. A Eur. J. 24 (2018) 12280–12290, doi:10.1002/chem.201801587.
[26] J. Ihonen, M. Mikkola, G. Lindbergh, Flooding of gas diffusion backing in PEFCs: physical and electrochemical characterization, J. Electrochem. Soc. 151 (2004) 1152–1161, doi:10.1149/1.1763138.
[27] A. Oyarce, N. Holmström, A. Bodén, C. Lagergren, G. Lindbergh, Operating conditions affecting the contact resistance of bi-polar plates in proton exchange membrane fuel cells, J. Power Sour. 231 (2013) 246–255, doi:10.1016/j.jpowsour.2012.12.100.
[28] J. Moulder, W. Stickle, P. Sobol, K. Bomben, Handbook of X-ray Photoelectron Spectroscopy, Perkin-Elmer Corp., Physical Electronics Division, Eden Prairie, Minnesota, USA, 1992, doi:10.1002/sia.740030412.
[29] A. Mesarwi, A. Ignatiev, X-ray photoemission study of Y-promoted oxidation of the Si(100) surface, Surf. Sci. 244 (1991) 15–21, doi:10.1016/0039-6028(91)90165-O.
[30] J.S. Kanady, P. Leidinger, A. Haas, S. Titlbach, S. Schunk, K. Schierle-Arndt, E.J. Crumlin, C.H. Wu, A.P. Alivisatos, Synthesis of Pt3Y and other early-late intermetallic nanoparticles by way of a molten reducing agent, J. Am. Chem. Soc. 139 (2017) 5672–5675, doi:10.1021/jacs.7b01366.
[31] R. Cui, L. Mei, G. Han, J. Chen, G. Zhang, Y. Quan, N. Gu, L. Zhang, Y. Fang, B. Qian, X. Jiang, Z. Han, Facile synthesis of nanoporous Pt-Y alloy with enhanced electrocatalytic activity and durability, Sci. Rep. 7 (2017) 1–10, doi:10.1038/srep41826.
[32] R. Brown, M. Vorokhta, I. Khalakhan, M. Dopita, T. Vonderach, T. Skála, N. Lindahl, I. Matolínová, H. Grönbeck, K.M. Neyman, V. Matolín, B. Wickman, Unraveling the surface chemistry and structure in highly active sputtered Pt3Y catalyst films for the oxygen reduction reaction, ACS Appl. Mater. Interface 12 (2020) 4454–4462, doi:10.1021/acsami.9b17817.
[33] S.P. Kowalczyk, N. Edelstein, F.R. McFeely, L. Ley, D.A. Shirley, X-ray photoemission spectra of the 4d levels in rare-earth metals, Chem. Phys. Lett. 29 (1974) 491–495, doi:10.1016/0009-2614(74)85076-1.
[34] A. Velázquez-Palenzuela, F. Masini, A.F. Pedersen, M. Escudero-Escribano, D. Deiana, P. Malacrida, T.W. Hansen, D. Friebel, A. Nilsson, I.E.L. Stephens, I. Chorkendorff, The enhanced activity of mass-selected PtxGd nanoparticles for oxygen electroreduction, J. Catal. 328 (2015) 297–307, doi:10.1016/j.jcat.2014.12.012.
[35] D. Raiser, J.P. Deville, Study of XPS photoemission of some gadolinium compounds, J. Electron. Spectrosc. Relat. Phenom. 57 (1991) 91–97 10.1016/0368-2048(91)85016-M.
[36] J.L.M. Rupp, T. Drobek, A. Rossi, L.J. Gauckler, Chemical analysis of spray pyrolysis Gadolinia-doped Ceria electrolyte thin films for solid oxide fuel cells, Chem. Mater. 19 (2007) 1134–1142, doi:10.1021/cm061449f.
[37] B.D. Padalia, W.C. Lang, P.R. Norris, L.M. Watson, D.J. Fabian, X-Ray photoelectron core-level studies of the heavy rare-earth metals and their oxides, Proc. R. Soc. Lond. A 425 (1989) 73–90.
[38] D.D. Sarma, C.N.R. Rao, XPES studies of oxides of second- and third-row transition metals including rare earths, J. Electron Spectrosc. Relat. Phenomena. 20 (1980) 25–45, doi:10.1016/0368-2048(80)85003-1.
[39] H. Yin, Y. Gao, H. Guo, C. Wang, C. Yang, Effect of B2O3 content and microstructure on Verdet constant of Tb_2O_3-doped GBSG magneto-optical glass, J. Phys. Chem. C. 122 (2018) 16894–16900, doi:10.1021/acs.jpcc.8b04989.
[40] S. Saini, H.S. Yaddanapudi, K. Tian, Y. Yin, D. Magginetti, A. Tiwari, Terbium ion doping in $Ca_3Co_4O_9$: a step towards high-performance thermoelectric materials, Sci. Rep. 7 (2017) 44621, doi:10.1038/srep44621.
[41] O. Diaz-Morales, T.J.P. Hersbach, C. Badan, A.C. Garcia, M.T.M. Koper, Hydrogen adsorption on nano-structured platinum electrodes, Faraday Discuss. 210 (2018) 301–315, doi:10.1039/c8fd00062j.
[42] D.F. Van Der Vliet, C. Wang, D. Li, A.P. Paulikas, J. Greeley, R.B. Rankin, D. Strmcnik, D. Tripkovic, N.M. Markovic, V.R. Stamenkovic, Unique electrochemical adsorption properties of Pt-skin surfaces, Angew. Chem. Int. Ed. 51 (2012) 3139–3142, doi:10.1002/anie.201107668.
[43] R. Chattot, I. Martens, M. Scohy, J. Herranz, J. Drnec, F. Maillard, L. Dubau, Disclosing Pt-bimetallic alloy nanoparticle surface lattice distortion with electrochemical probes, ACS Energy Lett. 5 (2020) 162–169, doi:10.1021/acsenergylett.9b02287.
[44] H.a. Gasteiger, S.S. Kocha, B. Sompalli, F.T. Wagner, Activity benchmarks and requirements for Pt, Pt-alloy, and non-Pt oxygen reduction catalysts for PEMFCs, Appl. Catal. B Environ. 56 (2005) 9–35, doi:10.1016/j.apcatb.2004.06.021.
[45] T. Daio, A. Staykov, L. Guo, J. Liu, M. Tanaka, S.Matthew Lyth, K. Sasaki, Lattice strain mapping of platinum nanoparticles on carbon and SnO_2 supports, Sci. Rep. 5 (2015) 1–10, doi:10.1038/srep13126.
[46] M. Escudero-Escribano, A. Verdaguer-Casadevall, P. Malacrida, U. Grønbjerg, B.P. Knudsen, A.K. Jepsen, J. Rossmeisl, I.E.L. Stephens, I. Chorkendorff, Pt5Gd as a highly active and stable catalyst for oxygen electroreduction, J. Am. Chem. Soc. 134 (2012) 16476–16479, doi:10.1021/ja306348d.
[47] I.E.L. Stephens, A.S. Bondarenko, L. Bech, I. Chorkendorff, Oxygen electroreduction activity and X-ray photoelectron spectroscopy of platinum and early transition metal alloys, ChemCatChem 4 (2012) 341–349, doi:10.1002/cctc.201100343.
[48] R. Chattot, O.Le Bacq, V. Beermann, S. Kühl, J. Herranz, S. Henning, L. Kühn, T. Asset, L. Guétaz, G. Renou, J. Drnec, P. Bordet, A. Pasturel, A. Eychmüller, T.J. Schmidt, P. Strasser, L. Dubau, F. Maillard, Surface distortion as a unifying concept and descriptor in oxygen reduction reaction electrocatalysis, Nat. Mater. 17 (2018) 827–833, doi:10.1038/s41563-018-0133-2.
[49] D.E. Newbury, N.W.M. Ritchie, Is scanning electron microscopy/energy dispersive X-ray spectrometry (SEM/EDS) quantitative? Scanning 35 (2013) 141–168, doi:10.1002/sca.21041.
[50] P. Malacrida, M. Escudero-Escribano, A. Verdaguer-Casadevall, I.E.L. Stephens, I. Chorkendorff, Enhanced activity and stability of Pt–La and Pt–Ce alloys for oxygen electroreduction: the elucidation of the active surface phase, J. Mater. Chem. A. 2 (2014) 4234, doi:10.1039/c3ta14574c.
[51] G. Topalov, G. Ganske, E. Lefterova, U. Schnakenberg, E. Slavcheva, Preparation and properties of thin Pt-Ir films deposited by dc magnetron co-sputtering, Int. J. Hydrog. Energy. 36 (2011) 15437–15445, doi:10.1016/j.ijhydene.2011.08.100.
[52] M. Oezaslan, F. Hasché, P. Strasser, Oxygen Electroreduction on PtCo 3, PtCo and Pt 3 Co Alloy nanoparticles for alkaline and acidic PEM fuel cells, J. Electrochem. Soc. 159 (2012) B394–B405, doi:10.1149/2.075204jes.